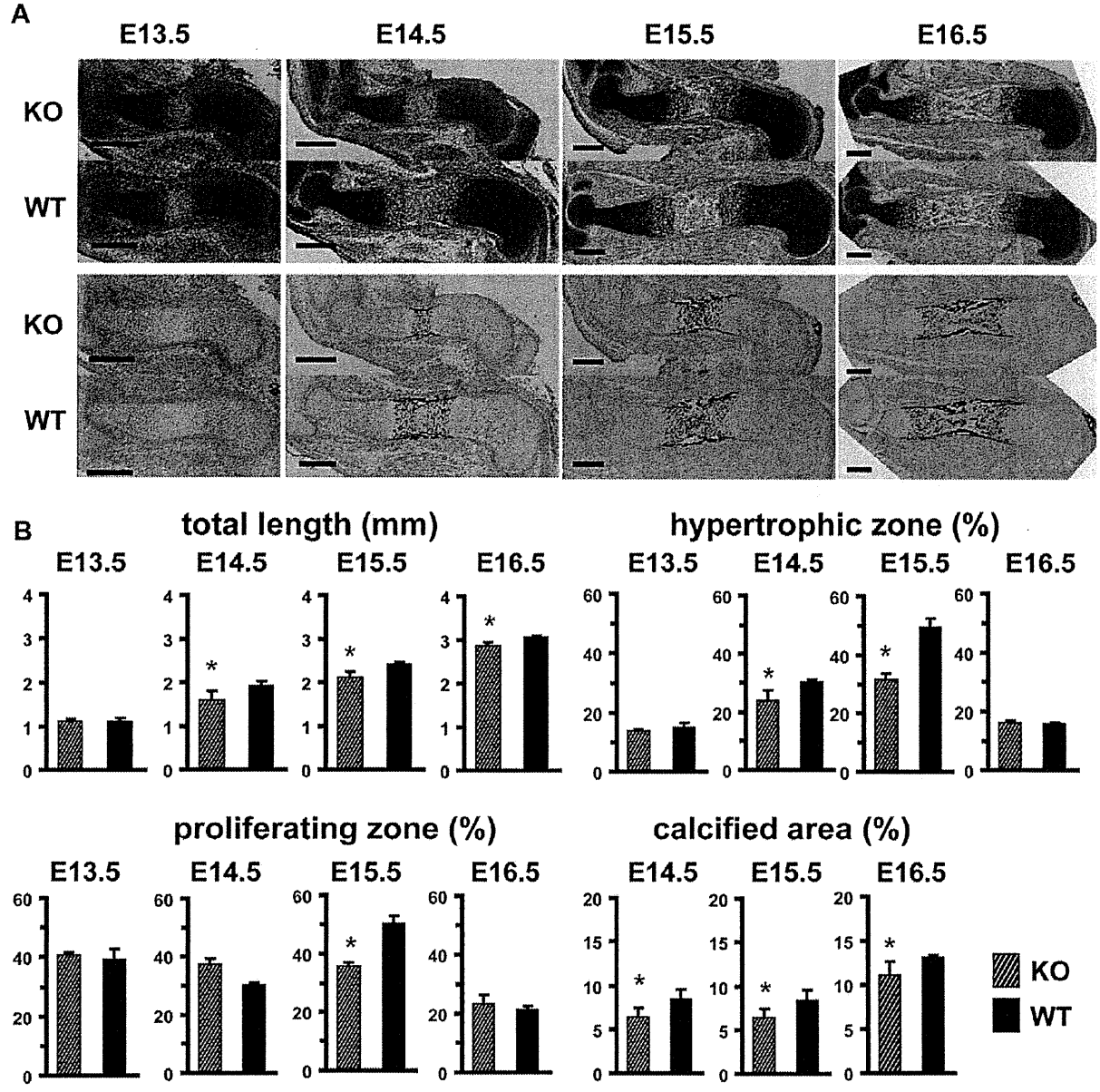

Figure 2. Growth of the embryonic humeri of SDF-1$^{-/-}$ mice delays. A: The embryonic humeri of wild-type (WT) and SDF-1$^{-/-}$ (KO) mice. Specimens were processed to paraffin-embedded sections and stained with hematoxylin, eosin (lower panels) and alcian blue (upper panels). **B**: Length of the humeri. The total length of the humeri and the ratios of the proliferating, the hypertrophic, or the calcified zone in each day were calculated as described in Methods section. Values are the mean and standard deviation of more than three independent experiments; *, $P<0.05$; Scale bar, 300 μm.
doi:10.1371/journal.pone.0037163.g002

SDF-1 Deficiency Impairs Type X Collagen Gene Expression

To examine the effect of SDF-1 to the phenotypical expression of type X collagen (Col X), and Sox9, metatarsal bones from E15.5 wild-type and SDF-1$^{-/-}$ mouse embryos were cultured with or without SDF-1 for 3 or 7 days, and total RNAs were extracted and quantified by real-time PCR.

The expression of Col X mRNA increased from day 3 to day 7 in untreated wild-type metatarsals (**Figure 6D**), which demonstrated the normal growth of the explant culture. The expression of Col X mRNA decreased significantly at day 7 in untreated SDF-1$^{-/-}$ metatarsals. The administration of recombinant SDF-1 to SDF-1$^{-/-}$ metatarsals recovered the expression of Col X. There was no statistically significant difference in Sox9 expression.

Furthermore, primary chondrocytes isolated from wild-type and SDF-1$^{-/-}$ mice were cultured for 3 weeks in chondrogenic medium supplemented with insulin to induce chondrocyte differentiation. Chondrocytes from SDF-1$^{-/-}$ mice showed decreased Col X expression compared with that from wild-type mice (**Figure 6E**). The expression of Sox9 showed no statistically significant difference.

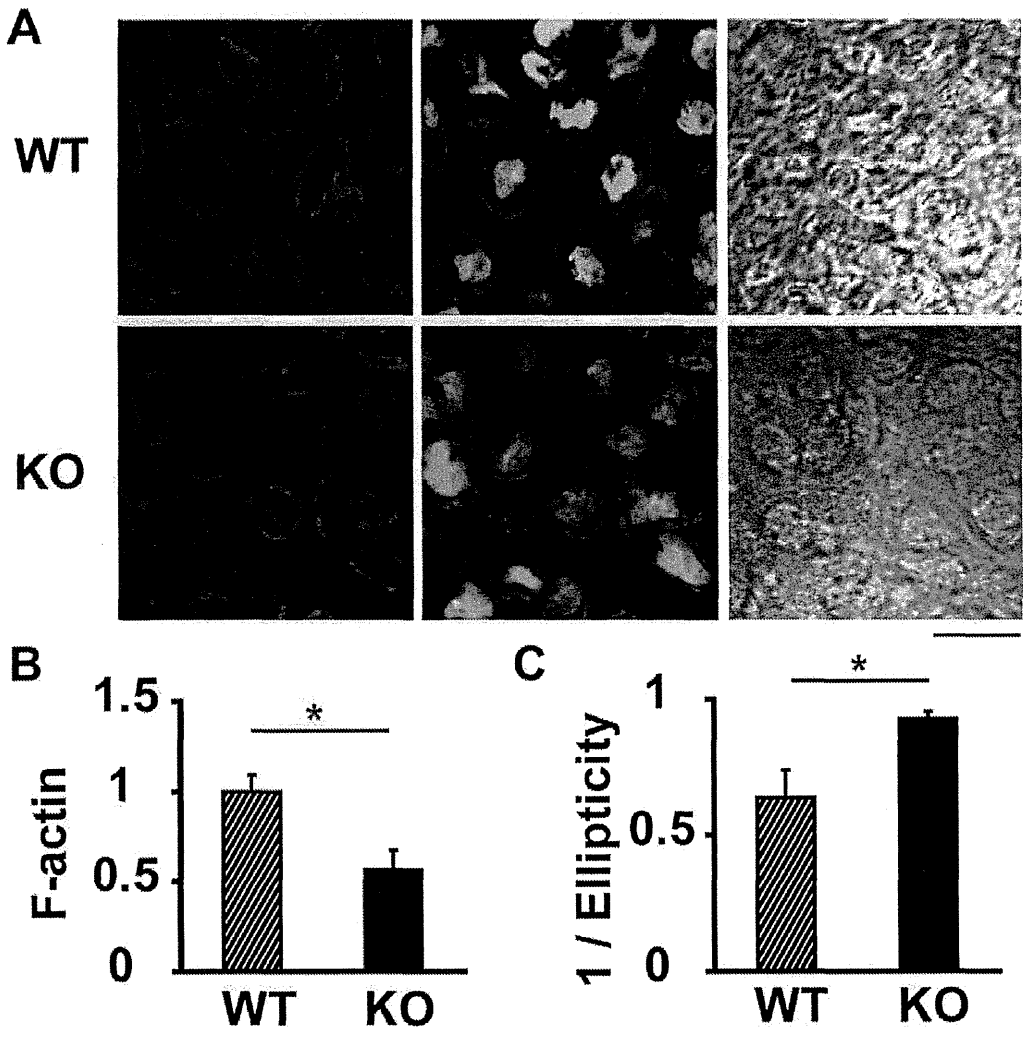

Figure 3. Cytoskeleton of hypertrophic chondrocytes in the humeri. A: Frozen sections of the humeri isolated from SDF-$1^{-/-}$ (KO), and wild-type (WT) mice at E15.5, were fixed with paraformaldehyde and stained with Rhodamine-Phalloidin for actin filaments and SYBR Green for nuclei. Left panel, Rhodamine-Phalloidin; middle panel, merge of Rhodamine-Phalloidin and SYBR Green; right panel, differentiation interference image. Representative fields are shown. **B**: The intensity of actin filament staining (F-actin) was quantified with Image J software. Values were normalized to F-actin of WT chondrocytes. **C**: The ratios of the short axis to the long axis (1/Ellipticity) in chondrocytes were calculated with Image J. Values are the mean and s.e.m. of more than three separate experiments; *, $P<0.05$; Scale bar, 10 μm.
doi:10.1371/journal.pone.0037163.g003

Discussion

SDF-1/CXCR4 plays important roles in the biological and physiological functions of MSCs [14,15], serving as a potent chemoattractant to recruit circulating or residing CXCR4-expressing MSCs to injured organs [16–21], including the fracture site of bones [22]. SDF-1 also plays crucial roles in the formation of multiple organ systems during embryogenesis [30–32], and it has been shown to associate with several diseases involving the skeleton, including rheumatoid arthritis and cancers that metastasize to the bone [33,34]. In the present study we showed, for the first time, the promotion of chondrocyte hypertrophy with SDF-1 and contribution of SDF-1 to the actin reorganization, which had been shown to be important for chondrocyte differentiation.

During the endochondral bone development, SDF-1 is expressed at the growth plate, but the precise localization of SDF-1 in the growth plate is controversial. A previous study showed that SDF-1 was expressed in the central region of the proliferating zone of the growth plate at E14.5 and it was expressed in the periosteum and central region of the proliferating zone at E16.5 [35]. On the other hand, another study showed that SDF-1 was expressed in the area adjacent to the hypertrophic zone of the growth plate [36]. Immunohistochemical analysis of the current study revealed that SDF-1 protein was expressed in hypertrophic chondrocytes of the growth plates of the tibia and the fracture callus (**Figure 1**) as well as the hypertrophic zone of mouse embryos (data not shown). These data suggest that SDF-1 has important, physiological roles in the hypertrophic zone during the endochondral bone formation even after birth.

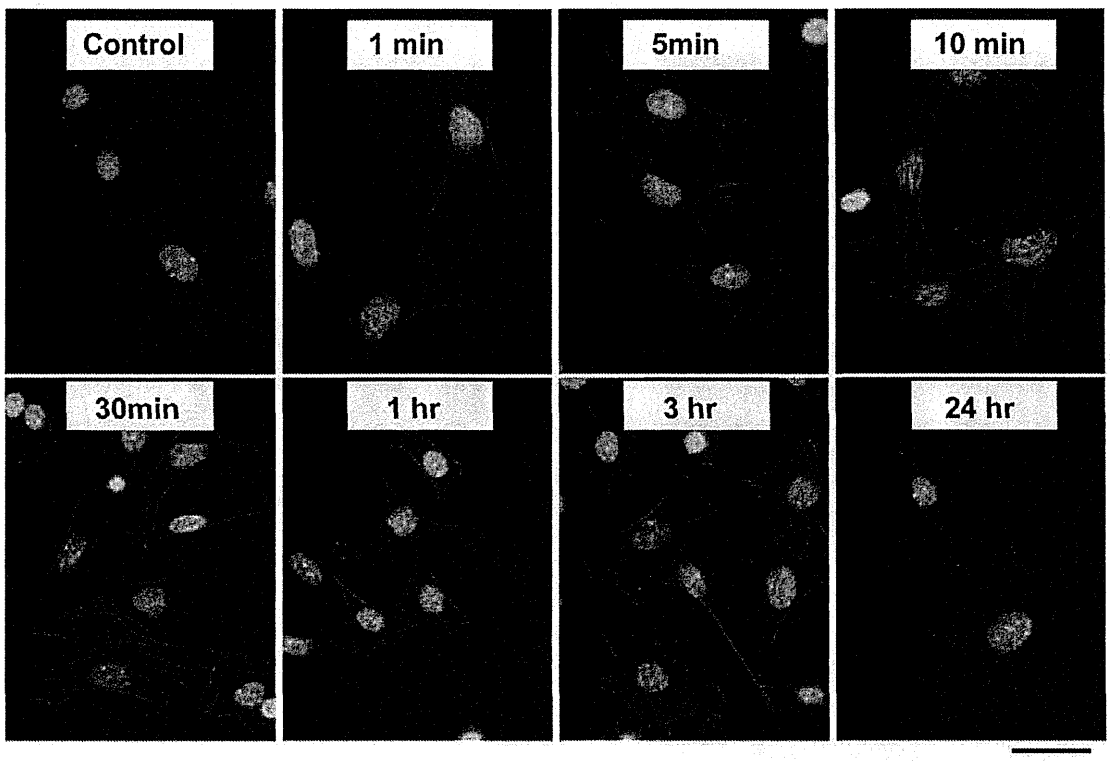

Figure 4. SDF-1 simulates actin assembly and stress fiber formation in a time-dependent manner. Primary chondrocytes from wild-type mice were treated with SDF-1 (100 ng/ml) as indicated. Cells were then fixed with paraformaldehyde and stained with Rhodamine-Phalloidin for actin filaments and 4′,6-diamidino-2-phenylindole for nuclei; Scale bar, 20 μm.
doi:10.1371/journal.pone.0037163.g004

SDF-1 is involved in the migration of hematopoietic progenitors and morphogenesis of leukocytes [37]. In the processes, SDF-1 induces morphological changes in adherent leukocytes and the acquisition of a bipolar shape with front leading edges [38,39], by stimulating the actin polymerization in a Rac and Cdc42-dependent fashion [38], and activating the small GTPases that control the actin cytoskeleton [40]. On the other hand, the actin cytoskeleton plays important roles in cellular homeostasis, proliferation and differentiation [41,42]. Even in the hypertrophic transition during chondrocyte differentiation, chondrocytes change the cell shape from a fibroblastoid to a round or polygonal morphology [23] and, as an upstream regulator of cytoskeletal dynamics, RhoA/ROCK signaling was shown to associate with chondrocyte hypertrophy [43]. In this study, incubation of wild-type and SDF-$1^{-/-}$ chondrocytes with SDF-1 changed the cell shape with an increase of F-actin density (**Figure 4**). In accordance with this fact, actin cytoskeletons of wild-type and SDF-$1^{-/-}$ hypertrophic chondrocytes in the humeri were different in the amount and the shape (**Figure 3**). These results suggest that SDF-1 signaling affects the reorganization of the actin cytoskeleton and the maintenance of the cellular morphology.

Phenotypic changes of SDF-$1^{-/-}$ hypertrophic chondrocytes of the humeri were mostly observed from E14.5 to E15.5, and the significant difference was lost at E16.5 (**Figure 2**). As we observed the vascularization of the humeri at E15.5 with the expression of SDF-1, we assume that the shortness of the humeri of SDF-$1^{-/-}$ mice is compensated by the effects of circulating factors from blood after neovascularization occurs. To exclude the effect of the vascularization of the humeri, the organ culture of metatarsal bones was performed, and we found that the bone growth was disturbed by lack of SDF-1, and that the discretion was rescued by the administration of SDF-1. These results suggest that SDF-1 is crucial in chondrocyte differentiation at the prevascularized stage, and the functions of SDF-1 in chondrocyte differentiation are totally apart from roles on the recruitment of MSCs nor HSCs.

The bone growth is driven primarily by the rate of production of hypertrophic chondrocytes from proliferating chondrocytes [44]. In the metatarsal explant culture, lack of SDF-1 resulted in the decreased expression of Col X with disturbance of the bone growth (**Figures 6A, D**). This fact suggests SDF-1 signaling is important for the hypertrophic conversion of proliferating chondrocytes. Interestingly, the appearance of the calcified zones was delayed in the explant culture of SDF-$1^{-/-}$ mice (**Figures 5B, C**). Since the hypertrophic conversion is a prerequisite of calcification of chondrocytes, SDF-1 is suggestively crucial on the hypertrophic conversion and the subsequent calcification of chondrocytes. Indeed, the delayed calcification was also found in the SDF-$1^{-/-}$ humeri (**Figure 2A**), and the disturbed hypertrophic conversion led to the shortness of calcified zones as well as that of the hypertrophic zones in SDF-$1^{-/-}$ mouse embryos (**Figure 2B**). Furthermore, the stimulation of SDF-1 to SDF-$1^{-/-}$ metatarsals increased the expression of Col X mRNA (**Figure 6D**). Since SDF-1 is expressed at prehypertrophic and hypertrophic chondrocytes (**Figure 1**) with CXCR4 expression being the strongest in the hypertophic chondrocytes [**36**], the effects of SDF-1 on chondrocyte differentiation may have occurred mainly in the prehypertrophic and hypertrophic zones as enhancement of chondrocyte hypertrophy.

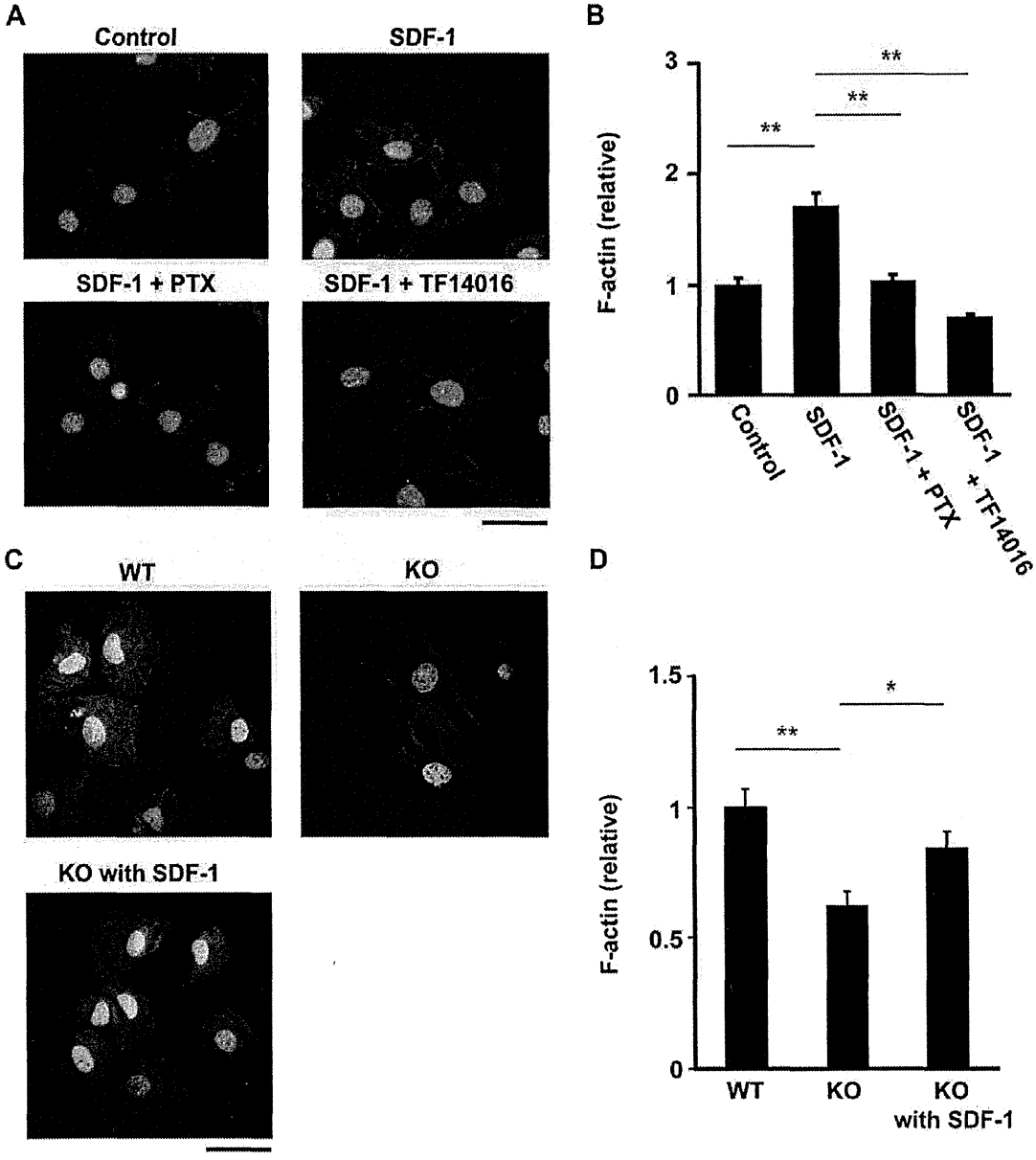

Figure 5. SDF-1/CXCR4 pathway controls actin cytoskeleton. A: Treatment with SDF-1 increased the actin filament density in primary chondrocytes. Primary chondrocytes from wild-type mice were treated with SDF-1 (100 ng/ml), or SDF-1 and CXCR4 specific antagonist, TF14016 (100 μM) or pertussis toxin (PTX, 100 ng/ml) for 60 m and stained with Rhodamine-Phalloidin. **B**: The F-actin content in chondrocytes was analyzed with Image J software. All values were normalized to F-actin of chondrocytes treated with conditioned medium only. **C**: Actin cytoskeleton of primary chondrocyte from SDF-$1^{-/-}$ (KO), and wild-type (WT) mice. **D**: The F-actin content in chondrocytes was quantified with Image J software. All values were normalized to the F-actin of wild-type chondrocyte. Values are the mean and s.e.m. of more than three separate experiments; *, $P<0.05$, **,$P<0.05$; Scale bar, 20 μm.
doi:10.1371/journal.pone.0037163.g005

However, the present study contains a few notable limitations. Firstly this study does not show the intracellular signaling of SDF-1 in chondrocyte differentiation. **Figure 5A** showed that formation of actin stress fibers in untreated wild-type chondrocytes and chondrocytes treated with SDF-1 and TF14016 was similar, but a slight actin stress fiber formation was observed in cells treated with SDF-1 and PTX. Since PTX inactivates Gi, actin stress fiber formation with SDF-1 and PTX may also have resulted from the increase of F-actin and contraction of actomyosin through G12/13. Actin stress fiber formation for the hypertrophic transition by SDF-1 may strongly depend on Gi in addition to G12/13. This result is compatible with a previous report that RhoA/ROCK signaling, downstream of G12/13, inhibited hypertrophic differentiation [43]. SDF-1 signal transduction pathway in chondrocytes is still elusive and remains to be investigated in the future.

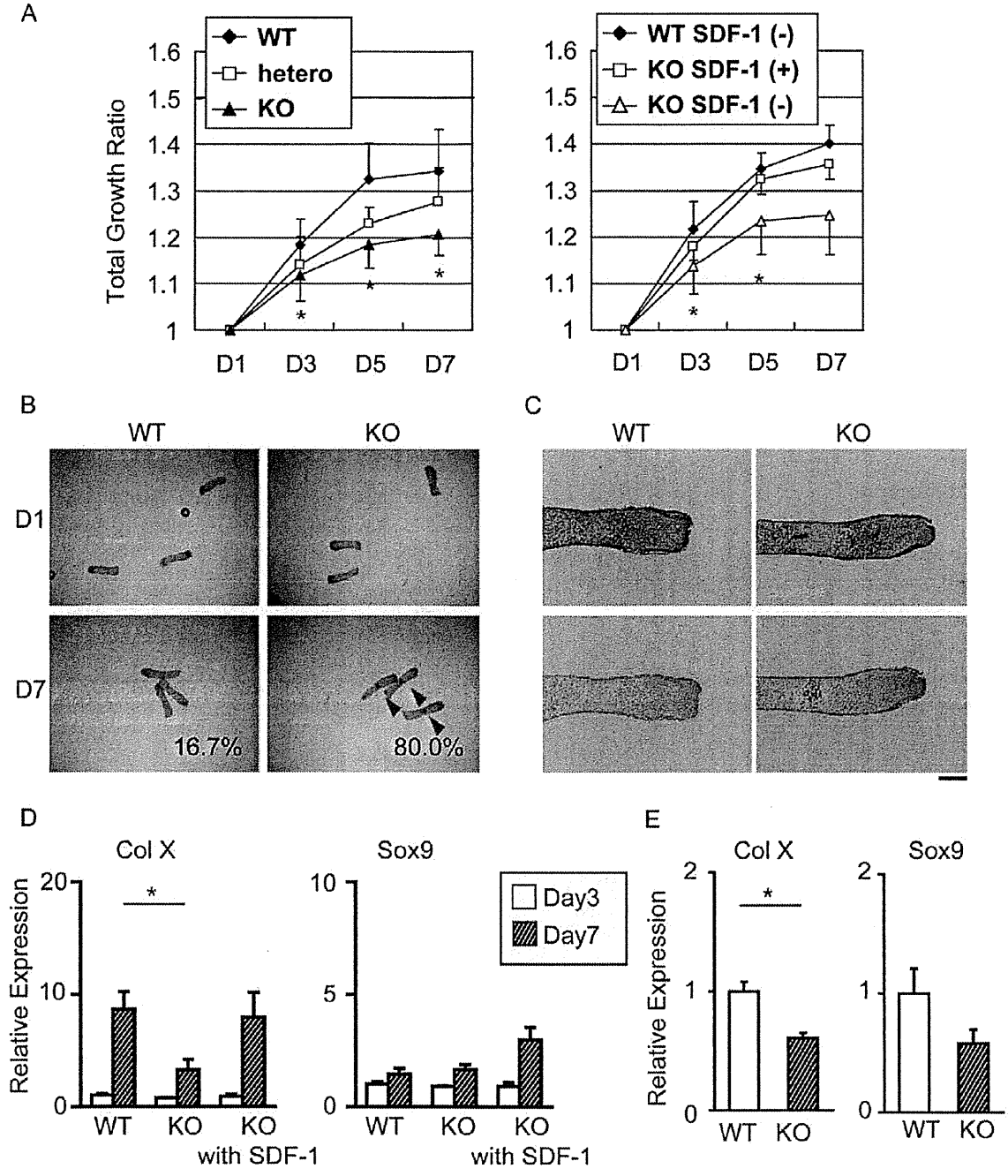

Figure 6. Lack of SDF-1 delays the growth metatarsals in organ culture. A: The metatarsal bones were harvested from SDF-1$^{-/-}$ (KO), SDF-1+/− (hetero), and wild-type (WT) mice at E15.5, cultured for 7 days, and the total length was measured at day 1, 3, 5, and 7. The length of metatarsal bones was calculated by day 1 as controls. **B**: Calcified spots (arrows) were counted in KO and WT metatarsals at day 1 and 7. **C**: Metatarsal bones were stained with hematoxylin and eosin (upper panel), or von Kossa (lower panel); Scale bar, 200 μm. **D**: The expression levels of type X collagen (Col X) and Sox9 of cultured metatarsal bones from E15.5 WT and KO mice at day 3 and 10 were quantified by real-time PCR. **E**: Primary chondrocytes isolated from WT and KO mice were cultured for 3 weeks in chondrogenic medium supplemented with insulin. The expression levels of Col X and Sox9 were quantified by real-time PCR. Values are the mean and s.e.m. of more than three independent experiments; *, P<0.05.
doi:10.1371/journal.pone.0037163.g006

Another relevant limitation of this study is that this study did not elucidate the association of SDF-1 signaling with other signaling molecules regulating the hypertrophic conversion of chondrocytes. RhoA/ROCK signaling, the only signaling shown to associate with actin organization during chondrogenesis, suppresses Sox9 expression [24]. Sox9 mRNA expression, however, did not show any significant difference between wild-type and SDF-1$^{-/-}$ metatarsals and primary chondrocytes in monolayer in this study

(**Figures 6D, E**). SDF-1 may regulate the hypertrophic conversion in chondrocytic differentiation and the bone growth without the involvement of Sox9, but this assumption requires further investigations.

In addition, the influence of genetic background of SDF-$1^{-/-}$ mice cannot completely be removed. As about half of SDF-$1^{-/-}$ mice start to die after E16.5 for unknown reasons, contamination of the dying embryos can affect the results. These dying embryos are easily distinguishable by their relatively small size and dark red color and we did not use these embryos for the experiments. However, there is still a possibility of the contamination. One of the solutions for this issue is the use of conditional knock-out mice. As there is no report showing mice that express Cre recombinase specifically in SDF-1-expressing prehypertrophic and/or hypertrophic chondrocytes, this issue should be pursued in the near future.

In conclusion, we investigated the role of SDF-1 in chondrocyte differentiation and revealed that SDF-1 stimulates bone growth by mediating chondrocyte hypertrophy and regulates actin polymerization.

Materials and Methods

Reagents

Recombinant mouse CXCL12/SDF-1α was purchased from R&D Systems (Minneapolis, MN). Pertussis toxin (PTX) was purchased from Sigma-Aldrich (St. Louis, MO).

Mice

All animal studies were conducted in accordance with principles by Kyoto University Committee of Animal Resources, based on International Guiding Principles for Biomedical Research Involving Animals. All procedures for this study were approved by Kyoto University Committee of Animal Resources (Permit Number: MedKyo 11260). The generation of SDF-$1^{-/-}$ mice has been previously described [45]. Heterozygotes were maintained and backcrossed more than 10 times with C57BL/6NCrSlc mice. Homozygous mutant embryos were present at the expected Mendelian ratios until E15.5, and about half of the SDF-$1^{-/-}$ embryos were dead at E18.5. The embryos that die within the uteri were slightly small in dark red color, and these were not used for the experiments.

Mouse Rib Fracture Model

Mouse rib fracture model was created using 6-week-old wild-type (C57BL/6NCrSlc) mice as previously described [46]. The mice were sacrificed at day 10 for histological analysis.

Histological Analysis and Measurement of the Ratios of Proliferating and Hypertrophic Chondrocytes

Specimens were processed to paraffin-embedded sections with a thickness of 5–7 μm, and stained with hematoxylin, eosin and alcian blue. The areas of proliferating and hypertrophic cartilages were measured by computer tracing as previously described [47]. Immunohistochemical analysis was performed to detect SDF-1 protein as previously described [22].

Visualization of Cytoskeleton in Hypertrophic Chondrocytes of the Humeri

The humeri of embryonic day 15.5 (E15.5) were isolated from wild-type embryos or crosses of SDF-$1^{+/-}$ mice. Samples were frozen in O.C.T. Compound (Sakura Finetek Japan, Tokyo, Japan). Tissues were cryosectioned at 12 μm, and briefly airdried. Sections were fixed with 4% paraformaldehyde for 20 m, followed by two washes in phosphate-buffered saline (PBS). The membranes were permeabilized with 0.5% Triton X-100/PBS solution for 20 m, and incubated in the dark for 2 h with 100 nM Rhodamine-Phalloidin (Cytoskelton, Denver, CO) and 0.01% SYBR Green I nucleic acid gel stain (Life Technologies, Carlsbad, CA). Images were taken with Nicon P-Eclipse C1 confocal microscopy equipped with objective lens 60X/1.40 oil.

Isolation and Culture of Primary Chondrocytes

Primary chondrocytes were isolated from embryonic ribs at E15.5 and cultured in Dulbecco's Modified Eagle Medium, which was regarded as post passage 0 (pp 0). When the cells became preconfluent, the cells were trypsinized and were passaged (pp 1). Cell suspensions at the cell concentration of 1×10*5 cells/ml were used for actin polymerization assay. Primary chondrocytes (pp 0) were also cultured for 3 weeks in chondrogenic medium supplemented with insulin (10 μg/ml), transferrin (5.5 μg/ml), and sodium selenite (5 ng/ml) (Sigma, St. Louis, MO) to induce chondrocyte differentiation, as previously described [48].

Actin Polymerization Assay of Primary Chondrocytes

To investigate the function of SDF-1, the cells were treated with SDF-1, TF14016, and/or PTX added to the medium for 1 m, 5 m, 10 m, 30 m, 1 h, 3 h, or 24 h. Then the cells were fixed with 4% paraformaldehyde for 10 m, and stained with 100 nM Rhodamine-Phalloidin and 0.05% 4′,6-diamidino-2-phenylindole for 30 s or 0.01% SYBR Green according to the manufacture's protocol. Images were taken Olympus IX70 laser microscopy or Nicon P-Eclipse C1 confocal microcopy, and analyzed with Image J as described before [49].

Metatarsal Organ Culture

Three central metatarsal rudiments were isolated from each hind limb of E15.5 embryos. Every three metatarsals from each limb were placed into each well of a 24-well plate containing 0.5 ml of organ culture medium as previously described [50]. The day of explant harvest was regarded as day 0 and the culture medium was replaced at day 1, and 4. SDF-1 were applied to the well containing the explants from the right hind limb, and the ones from the left hind limb were treated with culture medium alone as controls. Cultures were observed and photographed with an Olympus SZX 12 dissecting microscope at day 1, 3, 5, and 7. The cultured metatarsals were harvested at day 7 for histological procedure, and at day 3 or 7 for RNA extraction.

RNA Extraction and Quantitative Real-time PCR

Total RNA from cultured metatarsal bones were snap frozen in liquid nitrogen, homogenized, and extracted total RNA using High Pure RNA Tissue Kit (Roche Diagnostics, Penzberg, Germany). Total RNA from primary chondrocyte was extracted using High Pure RNA Isolation Kit (Roche Diagnostics). The RNA was reverse-transcribed and real-time quantitative PCR was performed using FastStart Universal SYBR Green Master (Roche Diagnostics) and ABI7500 (Life Technologies) according to the manufacturer's instructions. All of gene expression data were normalized against glyceraldehyde-3-phosphate dehydrogenase (GAPDH, forward primer, 5′- AGGTCGGTGTGAACG-GATTTG, and reverse primer 5′- TGTAGACCATGTAGTT-GAGGTCA). Expression patterns of Col X (forward primer, 5′-AGGCTACCTGGATCAGGCTTC, and reverse primer 5′-ACATTCTTTTCAGCCTACCTCC), and Sox9 mRNA (forward primer, 5′-GAGCCGGATCTGAAGAGGGA, and reverse

primer 5′- GCTTGACGTGTGGCTTGTTC) were also analyzed. Standard curve was generated by serially diluted plasmids containing PCR amplicon sequences. Plasmids were synthesized using pTAC-1 vector (BioDynamics Laboratory, Tokyo, Japan).

Proliferation Assay

BrdU incorporation was assessed by the cell proliferation ELISA Biotrack kit (Amersham Biosciences, Piscataway, NJ). BrdU was administrated into the mice at E15.5 2 h before the harvest. BrdU-positive cells were detected immunohistochemically as previously described [22].

Statistical Analysis

Data were analyzed with Student's t test. A p value less than 0.05 was considered statistically significant.

Supporting Information

Figure S1 BRd-U staining of embryonic humeri. A: BRd-U staining of embryonic humeri of wild-type (WT) and SDF-1$^{-/-}$ (KO) mice. Embryonic humeri of wild-type and SDF-1$^{-/-}$ mice were processed to paraffin-embedded sections and stained with Brd-U. B: The percentage of positive cells for BRd-U was calculated in WT and KO humeri.
(TIF)

Acknowledgments

We are grateful to Professor K. Tashiro (Kyoto Prefectural University of Medicine) for valuable advice on this work, and to Associate Professor Kosei Ijiri (Faculty of Medicine, Kagoshima University) for his generous help. We also thank Drs. T. Aoyama, R. Tsutsumi, K. Nishitani, and K. Yamamoto (Kyoto University Graduate School of Medicine) for their valuable technical assistance.

Author Contributions

Conceived and designed the experiments: T. Kitaori T. Nakamura HI. Performed the experiments: KM T. Kitaori ST MI T. Kasahara HS. Analyzed the data: KM T. Kitaori SO NW HY HI. Contributed reagents/materials/analysis tools: SO NW NF T. Nagasawa. Wrote the paper: KM T. Kitaori NW HI.

References

1. Karsenty G (2009) Regulation of Bone Formation. Annu Rev Cell Dev Biol. : 25, 629–48.
2. Baharina AV, Mollers U, Bittner K, Vischer P, Bruckner P (2001) Role of the subchondral vascular system in endochondral ossification: endothelial cell-derived proteinases derepress late cartilage differentiation in vitro. Matrix Biol 20: 205–213.
3. Karaplis AC, Luz A, Glowacki J, Bronson RT, Tybulewicz VL, et al. (1994) Lethal skeletal dysplasia from targeted disruption of the parathyroid hormone-related peptide gene. Genes Dev 8: 277–289.
4. Lanske B, Karaplis AC, Lee K, Luz A, Vortkamp A, et al. (1996) PTH/PTHrP receptor in early development and Indian hedgehog-regulated bone growth. Science 273: 663–666.
5. St-Jacques B, Hammerschmidt M, McMahon AP (1999) Indian hedgehog signaling regulates proliferation and differentiation of chondrocytes and is essential for bone formation. Genes Dev 13: 2072–2086.
6. Hartmann C, Tabin CJ (2000) Dual roles of Wnt signaling during chondrogenesis in the chicken limb. Development 127: 3141–3159.
7. Akiyama H, Lyons JP, Mori-Akiyama Y, Yang X, Zhang R, et al. (2004) Interactions between Sox9 and beta-catenin control chondrocyte differentiation. Genes Dev 18: 1072–1087.
8. Murakami S, Balmes G, McKinney S, Zhang Z, Givol D, et al. (2004) Constitutive activation of MEK1 in chondrocytes causes Stat1-independent achondroplasia-like dwarfism and rescues the Fgfr3-deficient mouse phenotype. Genes Dev 18: 290–305.
9. Tashiro K, Tada H, Heilker R, Shirozu M, Nakano T, et al. (1993) Signal sequence trap: a cloning strategy for secreted proteins and type I membrane proteins. Science 261: 600–603.
10. Nagasawa T, Kikutani H, Kishimoto T (1994) Molecular cloning and structure of a pre-B-cell growth-stimulating factor. Proc Natl Acad Sci U S A 91: 2305–2309.
11. Bleul CC, Farzan M, Choe H, Parolin C, Clark-Lewis I, et al. (1996) The lymphocyte chemoattractant SDF-1 is a ligand for LESTR/fusin and blocks HIV-1 entry. Nature 382: 829–833.
12. Hartmann TN, Grabovsky V, Pasvolsky R, Shulman Z, Buss EC, et al. (2008) A crosstalk between intracellular CXCR7 and CXCR4 involved in rapid CXCL12-triggered integrin activation but not in chemokine-triggered motility of human T lymphocytes and CD34+ cells. J Leukoc Biol 84: 1130–1140.
13. Levoye A, Balabanian K, Baleux F, Bachelerie F, Lagane B (2009) CXCR7 heterodimerizes with CXCR4 and regulates CXCL12-mediated G protein signaling. Blood 113: 6085–6093.
14. Wynn RF, Hart CA, Corradi-Perini C, O'Neill L, Evans CA, et al. (2004) A small proportion of mesenchymal stem cells strongly expresses functionally active CXCR4 receptor capable of promoting migration to bone marrow. Blood 104: 2643–2645.
15. Dar A, Goichberg P, Shinder V, Kalinkovich A, Kollet O, et al. (2005) Chemokine receptor CXCR4-dependent internalization and resecretion of functional chemokine SDF-1 by bone marrow endothelial and stromal cells. Nat Immunol 6: 1038–1046.
16. Kucia M, Ratajczak J, Reca R, Janowska-Wieczorek A, Ratajczak MZ (2004) Tissue-specific muscle, neural and liver stem/progenitor cells reside in the bone marrow, respond to an SDF-1 gradient and are mobilized into peripheral blood during stress and tissue injury. Blood Cells Mol Dis 32: 52–57.
17. Abbott JD, Huang Y, Liu D, Hickey R, Krause DS, et al. (2004) Stromal cell-derived factor-1alpha plays a critical role in stem cell recruitment to the heart after myocardial infarction but is not sufficient to induce homing in the absence of injury. Circulation 110: 3300–3305.
18. Ma J, Ge J, Zhang S, Sun A, Shen J, et al. (2005) Time course of myocardial stromal cell-derived factor 1 expression and beneficial effects of intravenously administered bone marrow stem cells in rats with experimental myocardial infarction. Basic Res Cardiol 100: 217–223.
19. Ji JF, He BP, Dheen ST, Tay SS (2004) Interactions of chemokines and chemokine receptors mediate the migration of mesenchymal stem cells to the impaired site in the brain after hypoglossal nerve injury. Stem Cells 22: 415–427.
20. Togel F, Isaac J, Hu Z, Weiss K, Westenfelder C (2005) Renal SDF-1 signals mobilization and homing of CXCR4-positive cells to the kidney after ischemic injury. Kidney Int 67: 1772–1784.
21. Avniel S, Arik Z, Maly A, Sagie A, Basst HB, et al. (2006) Involvement of the CXCL12/CXCR4 pathway in the recovery of skin following burns. J Invest Dermatol 126: 468–476.
22. Kitaori T, Ito H, Schwarz EM, Tsutsumi R, Yoshitomi H, et al. (2009) Stromal cell-derived factor 1/CXCR4 signaling is critical for the recruitment of mesenchymal stem cells to the fracture site during skeletal repair in a mouse model. Arthritis Rheum 60: 813–823.
23. von der Mark K, von der Mark H (1977) Immunological and biochemical studies of collagen type transition during in vitro chrondrogenesis of chick limb mesodermal cells. J Cell Biol 73: 736–747.
24. Woods A, Wang G, Beier F (2005) RhoA/ROCK signaling regulates Sox9 expression and actin organization during chondrogenesis. J Biol Chem 280: 11626–11634.
25. Woods A, Beier F (2006) RhoA/ROCK signaling regulates chondrogenesis in a context-dependent manner. J Biol Chem 281: 13134–13140.
26. Kumar D, Lassar AB (2009) The transcriptional activity of Sox9 in chondrocytes is regulated by RhoA signaling and actin polymerization. Mol Cell Biol 29: 4262–4273.
27. Alsayed Y, Ngo H, Runnels J, Leleu X, Singha UK, et al. (2007) Mechanisms of regulation of CXCR4/SDF-1 (CXCL12)-dependent migration and homing in multiple myeloma. Blood 109: 2708–2717.
28. Azab AK, Azab F, Blotta S, Pitsillides CM, Thompson B, et al. (2009) RhoA and Rac1 GTPases play major and differential roles in stromal cell-derived factor-1-induced cell adhesion and chemotaxis in multiple myeloma. Blood 114: 619–629.
29. Tamamura H, Hiramatsu K, Mizumoto M, Ueda S, Kusano S, et al. (2003) Enhancement of the T140-based pharmacophores leads to the development of more potent and bio-stable CXCR4 antagonists. Org Biomol Chem 1: 3663–3669.
30. Raz E, Mahabaleshwar H (2009) Chemokine signaling in embryonic cell migration: a fisheye view. Development 136: 1223–1229.
31. Tachibana K, Hirota S, Iizasa H, Yoshida H, Kawabata K, et al. (1998) The chemokine receptor CXCR4 is essential for vascularization of the gastrointestinal tract. Nature 393: 591–594.
32. Zou YR, Kottmann AH, Kuroda M, Taniuchi I, Littman DR (1998) Function of the chemokine receptor CXCR4 in haematopoiesis and in cerebellar development. Nature 393: 595–599.
33. Grassi F, Cristino S, Toneguzzi S, Piacentini A, Facchini A, et al. (2004) CXCL12 chemokine up-regulates bone resorption and MMP-9 release by

human osteoclasts: CXCL12 levels are increased in synovial and bone tissue of rheumatoid arthritis patients. J Cell Physiol 199: 244–251.
34. Sun YX, Schneider A, Jung Y, Wang J, Dai J, et al. (2005) Skeletal localization and neutralization of the SDF-1(CXCL12)/CXCR4 axis blocks prostate cancer metastasis and growth in osseous sites in vivo. J Bone Miner Res 20: 318–329.
35. Jung Y, Wang J, Schneider A, Sun YX, Koh-Paige AJ, et al. (2006) Regulation of SDF-1 (CXCL12) production by osteoblasts; a possible mechanism for stem cell homing. Bone 38: 497–508.
36. Wei L, Kanbe K, Lee M, Wei X, Pei M, et al. (2010) Stimulation of chondrocyte hypertrophy by chemokine stromal cell-derived factor 1 in the chondro-osseous junction during endochondral bone formation. Dev Biol 341: 236–245.
37. Doitsidou M, Reichman-Fried M, Stebler J, Koprunner M, Dorries J, et al. (2002) Guidance of primordial germ cell migration by the chemokine SDF-1. Cell 111: 647–659.
38. Vicente-Manzanares M, Viton M, Sanchez-Madrid F (2004) Measurement of the levels of polymerized actin (F-actin) in chemokine-stimulated lymphocytes and GFP-coupled cDNA transfected lymphoid cells by flow cytometry. Methods Mol Biol 239: 53–68.
39. van Buul JD, Voermans C, van Gelderen J, Anthony EC, van der Schoot CE, et al. (2003) Leukocyte-endothelium interaction promotes SDF-1-dependent polarization of CXCR4. J Biol Chem 278: 30302–30310.
40. Vicente-Manzanares M, Cabrero JR, Rey M, Perez-Martinez M, Ursa A, et al. (2002) A role for the Rho-p160 Rho coiled-coil kinase axis in the chemokine stromal cell-derived factor-1alpha-induced lymphocyte actomyosin and microtubular organization and chemotaxis. J Immunol 168: 400–410.
41. Watanabe N (2010) Inside view of cell locomotion through single-molecule: fast F-/G-actin cycle and G-actin regulation of polymer restoration. Proc Jpn Acad Ser B Phys Biol Sci 86: 62–83.
42. Saltel F, Chabadel A, Bonnelye E, Jurdic P (2008) Actin cytoskeletal organisation in osteoclasts: a model to decipher transmigration and matrix degradation. Eur J Cell Biol 87: 459–468.
43. Wang G, Woods A, Sabari S, Pagnotta L, Stanton LA, et al. (2004) RhoA/ROCK signaling suppresses hypertrophic chondrocyte differentiation. J Biol Chem 279: 13205–13214.
44. Kronenberg HM (2003) Developmental regulation of the growth plate. Nature 423: 332–336.
45. Nagasawa T, Hirota S, Tachibana K, Takakura N, Nishikawa S, et al. (1996) Defects of B-cell lymphopoiesis and bone-marrow myelopoiesis in mice lacking the CXC chemokine PBSF/SDF-1. Nature 382: 635–638.
46. Ito H, Akiyama H, Shigeno C, Iyama K, Matsuoka H, et al. (1999) Hedgehog signaling molecules in bone marrow cells at the initial stage of fracture repair. Biochem Biophys Res Commun 262: 443–451.
47. Ito H, Koefoed M, Tiyapatanaputi P, Gromov K, Goater JJ, et al. (2005) Remodeling of cortical bone allografts mediated by adherent rAAV-RANKL and VEGF gene therapy. Nat Med 11: 291–297.
48. Fukai A, Kawamura N, Saito T, Oshima Y, Ikeda T, et al. (2010) Akt1 in murine chondrocytes controls cartilage calcification during endochondral ossification under physiologic and pathologic conditions. Arthritis Rheum 62: 826–836.
49. Stein CA, Wu S, Voskresenskiy AM, Zhou JF, Shin J, et al. (2009) G3139, an anti-Bcl-2 antisense oligomer that binds heparin-binding growth factors and collagen I, alters in vitro endothelial cell growth and tubular morphogenesis. Clin Cancer Res 15: 2797–2807.
50. Alvarez J, Sohn P, Zeng X, Doetschman T, Robbins DJ, et al. (2002) TGFbeta2 mediates the effects of hedgehog on hypertrophic differentiation and PTHrP expression. Development 129: 1913–1924.

Rheumatol Int (2012) 32:3869–3874
DOI 10.1007/s00296-011-2283-2

ORIGINAL ARTICLE

Objective assessment of abnormal gait in patients with rheumatoid arthritis using a smartphone

Minoru Yamada · Tomoki Aoyama · Shuhei Mori · Shu Nishiguchi · Kazuya Okamoto · Tatsuaki Ito · Shinyo Muto · Tatsuya Ishihara · Hiroyuki Yoshitomi · Hiromu Ito

Received: 2 August 2011 / Accepted: 10 December 2011 / Published online: 23 December 2011
© Springer-Verlag 2011

Abstract A disturbance in gait pattern is a serious problem in patients with rheumatoid arthritis (RA). The aim of the present study was to examine the utility of the smartphone gait analysis application in patients with RA. The smartphone gait analysis application was used to assess 39 patients with RA (age 65.9 ± 10.0 years, disease duration 11.9 ± 9.4 years) and age-matched control individuals (mean age, 69.1 ± 5.8 years). For all RA patients, the following data were obtained: disease activity score (DAS) 28, modified health assessment questionnaire (mHAQ), and assessment of walking ability. Patients walked 20 m at their preferred speed, and trunk acceleration was measured using a Smartphone. After signal processing, we calculated the following gait parameters for each measurement terminal: peak frequency (PF), autocorrelation peak (AC), and coefficient of variance (CV) of the acceleration peak intervals. The gait parameters of RA and control groups were compared to examine the comparability of the 2 groups. Criterion-related validity was determined by evaluating the correlation between gait parameters and clinical parameters using Spearman's correlation coefficient. The RA group showed significantly lower scores for the walking speed, AC, and CV than the control group. There were no significant differences in PF. PF (gait cycle) was mildly associated with gait speed ($P < 0.05$). AC (gait balance) was moderately associated with the DAS, mHAQ, gait ability, and gait speed ($P < 0.05$). CV (gait variability) was moderately associated with the DAS, gait ability, and gait speed ($P < 0.05$). This is the first study to examine the use of a smartphone device for gait pattern measurement. The results suggest that some gait parameters recorded using the smartphone represent an acceptable assessment tool for gait in patients with RA.

Keywords Smartphone · Gait analysis · Validity · Rheumatoid arthritis

M. Yamada (✉) · T. Aoyama · S. Mori · S. Nishiguchi
Human Health Sciences, Graduate School of Medicine, Kyoto University, 53 Kawahara-cho, Shogoin, Sakyo-ku, Kyoto 606-8507, Japan
e-mail: yamada@hs.med.kyoto-u.ac.jp

K. Okamoto
Department of Medical Informatics, Kyoto University Hospital, Kyoto, Japan

T. Ito · S. Muto
NTT Cyber Solutions Laboratories, Yokosuka, Japan

T. Ishihara
Nippon Telegraph and Telephone East Corporation, Sapporo, Japan

H. Yoshitomi
Department of Orthopaedic Surgery, Graduate School of Medicine, Kyoto University, Kyoto, Japan

H. Ito
Department for the Control of Rheumatic Diseases, Graduate School of Medicine, Kyoto University, Kyoto, Japan

Introduction

Rheumatoid arthritis (RA) affects approximately 1% of adults and has been recognised as one of the most critical rheumatological conditions in the developed world [1], largely because of the associated joint damage, decline in functional status, and premature mortality [2]. The disease process leads to chronic and progressive inflammation involving multiple joints as well as other organ systems, and RA is associated with substantial disability and

economic losses [3], and even reduces life expectancy [4]. Treatment comprises medication to control inflammation and multidisciplinary interventions to reduce symptoms and maximise self-management [5].

RA leads to functional disability and possible changes in normal gait pattern, a common but clinically serious problem that substantially affects quality of life in RA patients [6]. Previous studies have demonstrated that RA may lead to a decreased walking speed [7], shortened stride length, and increased double-stance period [8], indicative of a limitation in lower limb function. Because of day-to-day variations in inflammatory activity and gait pattern in RA patients, self-monitoring and self-management becomes very important for controlling abnormal gait.

Recently, wireless tri-axial accelerometers have become widely used for gait analysis, because they are easy to use, are inexpensive, and do not require a laboratory environment. Several authors have performed gait assessment using such accelerometers in a clinical setting, including in patients with stroke, patients with Parkinson's disease, and older adults [9–11]. More recently, LeMoyne et al. [12] performed gait analysis experiments using a Smartphone, which demonstrated a capacity to accurately quantify gait parameters with a sufficient level of consistency. Similarly, our previous research showed that the smartphone gait analysis application has the capacity to quantify gait parameters with a degree of accuracy that is comparable to that of tri-axial accelerometers [Nishiguchi et al. unpublished observation].

The simplicity and portability of the smartphone application permits gait self-assessment by concerned individuals in a non-clinical setting. The aim of the present study was to examine the utility of the smartphone gait analysis application in patients with RA.

Methods

Participants

This was a cross-sectional study performed between April 2011 and May 2011 in the rheumatology outpatient clinics of Kyoto University Hospital. A total of 39 RA patients (mean age, 65.9 ± 10.0 years) participated. Patients with RA defined by the American College of Rheumatology 1987 criteria were included. The patients were assessed by an experienced rheumatologist. We excluded participants based on the following exclusion criteria: other musculoskeletal disorders, cognitive disorders, Parkinson's disease, stroke, or unable to walk unassisted over 15 m using current walking aids. Twenty older individuals (mean age, 69.1 ± 5.8 years) also took part in this experiment as control participants. We obtained written informed consent from each participant in accordance with the guidelines approved by the Kyoto University Graduate School of Medicine and the Declaration of Human Rights, Helsinki, 1975.

RA evaluation

For all patients, the following data were obtained: disease activity score (DAS) 28, modified health assessment questionnaire (mHAQ), and assessment of walking ability.

The DAS includes 4 parameters: number of joints tender to touch (out of 28 joints), number of swollen joints (out of 28 joints), C-reactive protein level, and patient-assessed disease activity using a 100-mm visual analogue scale. The DAS is generally accepted as a reliable, valid, and responsive measure of disease activity in patients with RA [13].

The mHAQ is a self-reported measure of physical function. The mHAQ is a widely used and validated tool to quantify functional disability in RA [14]. The mHAQ disability index assesses 20 daily living activities, including dressing and grooming, rising, eating, walking, hygiene, reach, grip, and community activities. The mHAQ is expressed on a scale ranging from 0 to 3 (where 0 = no functional disability and 3 = severe functional disability).

Assessment of walking ability was based on a subscale of the RA foot and ankle scale, which is expressed on a scale ranging from 0 to 20 (where 0 = unable to walk and 20 = no limitation) [15].

Gait analysis system

The smartphone (size: 63-mm width, 119-mm height, 13.1-mm depth; weight: 139 g; Xperia SO-01B; Android 2.1; Sony Ericsson Mobile Communications Japan, Inc.) used in this study includes an acceleration sensor, a recording device, and a computer program for processing the acceleration signals. Trunk linear accelerations were measured using the smartphone while the subject walked on the walkway. The smartphone was attached to the L3 spinous process using a semi-elastic belt (Fig. 1). Before measurements, the accelerometer of the smartphone was calibrated statically against gravity. The accelerometer of the smartphone sampled at 33 Hz. The recorded signals were analysed by the application developed in the android environment.

Gait analysis

The participants were instructed to walk on a 20-m walkway at their preferred speed. All participants wore their usual walking shoes, avoiding high heels and hard-soled shoes. The mid (10-m) walking time was measured using an electronic stopwatch.

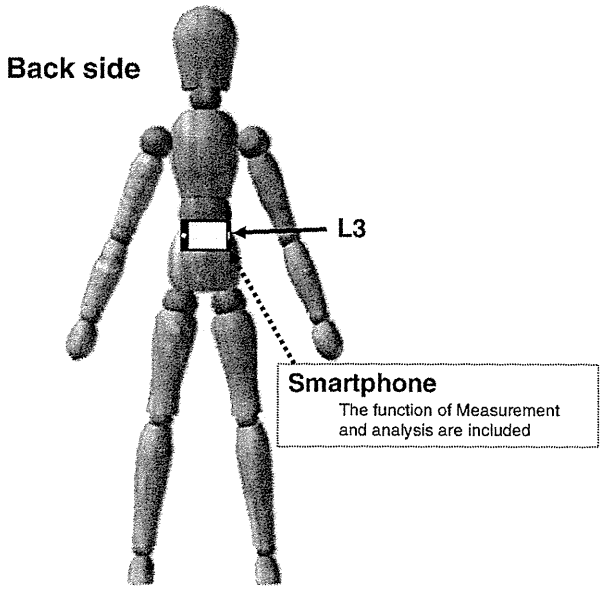

Fig. 1 Schematic representation of the use of the Smartphone, which was attached to the L3 spinous process, for gait assessment

Data processing

A period of steady state walking of 7.75 s was selected from the recording of each subject. This period contained about 256 acceleration measurements. We calculated the following gait parameters, according to previous studies: peak frequency (PF) [16], autocorrelation peak (AC) [16, 17], and coefficient of variance (CV) of the acceleration peak intervals [18, 19].

The PF value indicates the gait cycle, which is the time taken to take 1 step. The AC value indicates the degree of gait balance; the higher the AC value, the greater is the degree of balance. The CV value indicates the degree of gait variability, i.e., the variability in the elapsed time between the first contact of 2 consecutive footfalls. For calculating the gait parameters, we used the absolute values of the tri-axial acceleration data to decrease the influence of the measurement terminal posture. Let $a_{t_1:t_n} = a_{t_1}, a_{t_2}, \ldots, a_{t_n}$ denote the set of all acceleration absolute values acquired from time t_1 to t_n, for $t_1 \leq t_n$. Let a_t and n denote, respectively, the acceleration absolute value at time t and the number of all acceleration absolute values acquired from time t_1 to t_n.

PF f_p of acceleration data $a_{t_1:t_n}$ was detected with high accuracy based on the PF candidate f'_p, which was detected from the smoothed acceleration data in order to decrease the influence of the high-frequency measurement noise that accompanies PF detection. First, acceleration data $a_{t_1:t_n}$ was smoothed using a low-pass filter. Second, the PF candidate, f'_p, was detected where the power spectrum at frequency f'_p was the highest peak in the frequency space to which the smoothed acceleration data was converted by fast Fourier transformation. Finally, PF f_p was detected in the frequency space to which acceleration data $a_{t_1:t_n}$ was converted, where the power spectrum of PF f_p had the highest peak around PF candidate f'_p. The test–retest reliability using the inter-trial correlation coefficient (ICC 1.1) was 0.906 [Nishiguchi et al. unpublished observation].

AC R_p from the autocorrelation function was detected using PF f_p. This allowed us to detect AC R_p with a high degree of accuracy, based on the hypothesis that the gait cycle is related to the time lag when AC is detected [17]. The AC detection method was as follows: first, the autocorrelation function was calculated from acceleration data $a_{t_1:t_n}$. The autocorrelation function is represented by the sequence of the autocorrelation coefficients $R_{xx}(k)$ over increasing time lags k:

$$R_{xx}(k) = \frac{1}{n-k}\sum_{i=1}^{n-k} x_{t_i} x_{t_{i+k}} \quad (1)$$

Here, let x_t denote the normalised acceleration data, which are calculated by both the mean a_{MEAN} and standard deviation a_{SD} of acceleration data $a_{t_1:t_n}$; that is, $x(t) = a(t) - a_{\mathrm{MEAN}}/a_{\mathrm{SD}}$. Let n denote the number of acceleration data samples in our gait analysis. Finally, AC R_p was detected as the highest peak around the lag related to gait cycle T. The test–retest reliability using the ICC 1.1 was 0.752 [Nishiguchi et al. unpublished observation].

Coefficient of variance was calculated by using the group of positive peak time candidates detected in the smoothed acceleration data; this decreases the influence of the high-frequency measurement noise that accompanies positive peak detection. Here, the positive peak indicates the acceleration data with a positive convex shape on the acceleration waveform. First, acceleration data $a_{t_1:t_n}$ was smoothed using a low-pass filter. Second, each positive peak on the smoothed acceleration waveform was detected as a group of positive peak candidates. These measured times were extracted as a group of positive peak time candidates. Third, each positive peak of acceleration data $a_{t_1:t_n}$ was detected where each peak was the highest around each positive peak time candidate on the acceleration waveform. The time intervals between the neighbouring positive peaks were then calculated. Finally, CV is calculated from the mean t_{MEAN} and standard deviation t_{SD} of time intervals, as follows:

$$\frac{t_{\mathrm{SD}}}{t_{\mathrm{MEAN}}} \quad (2)$$

The test–retest reliability using the ICC 1.1 was 0.752 [Nishiguchi et al. unpublished observation].

Statistical analysis

Characteristics of RA and control groups were compared to examine the comparability of the 2 groups. Differences in the demographic variables and gait parameters between the 2 groups were analysed using the Student's t test or Chi-square test.

Criterion-related validity was determined by evaluating the correlation between gait parameters (PF, AC, and CV) and clinical parameters (DAS, mHAQ, walking ability, and walking speed) using Spearman's correlation coefficient in RA group. A multivariate analysis by means of multiple regression using a stepwise method was performed to investigate which of the gait parameters was independently associated with each clinical parameter in RA group. Data were entered and analysed using the SPSS program (Windows version 18.0, SPSS, Inc., Chicago, IL). A P value of <0.05 was considered statistically significant for all analyses.

Results

Characteristics of the participants are reported in Table 1. Typical acceleration waveforms are shown in Fig. 2.

Participants in the RA and control groups were comparable and well matched with regard to their baseline characteristics. There were no significant differences in age, body weight, height, or gender ($P > 0.05$). The RA group showed significantly lower scores for the walking speed, AC, and CV than the control group. There were no significant differences in PF (Table 1).

To determine the association between gait parameters and clinical parameters, we analysed Spearman's correlation coefficients (Table 2). PF was correlated with walking speed ($r = 280$, $P < 0.05$). AC was correlated with the DAS ($r = -0.283$, $P < 0.05$), mHAQ ($r = -0.368$, $P < 0.05$), and walking speed ($r = -0.704$, $P < 0.01$). CV was correlated with the DAS ($r = 0.334$, $P < 0.05$), walking ability ($r = -0.420$, $P < 0.01$), and walking speed ($r = 0.608$, $P < 0.01$). Walking speed was correlated with the mHAQ ($r = -0.442$, $P < 0.01$) and walking ability ($r = 0.413$, $P < 0.01$).

Stepwise regression analysis revealed that AC ($\beta = -0.435$, $P < 0.05$) was a significant and independent determinant of the DAS ($R^2 = 0.189$, $P < 0.05$). AC ($\beta = -0.368$, $P < 0.05$) was also a significant and independent determinant of the mHAQ ($R^2 = 0.135$, $P < 0.05$). CV ($\beta = -0.420$, $P < 0.05$) was a significant and independent determinant of the DAS ($R^2 = 0.232$, $P < 0.01$). PF ($\beta = -0.575$, $P < 0.01$) and AC ($\beta = -0.410$, $P < 0.01$) were significant and independent determinants of the DAS ($R^2 = 0.647$, $P < 0.01$) (Table 3).

Discussion

The results of the current study indicate that the RA group showed significantly lower scores for the gait parameters than the control group. Moreover, the clinical parameters were moderately associated with gait parameters recorded by a smartphone in patients with RA. We used the DAS, mHAQ, walking ability, and walking time as reference tools. The DAS index in RA patients reflects disease activity [13], and the mHAQ is often used for functional assessment in RA patients [14]. In this study, the DAS (disease activity) was associated with gait balance. The mHAQ (function) was also associated with gait balance. Further, walking ability was associated with gait variability, and walking speed was moderately associated with gait cycle and gait balance. Lelas et al. [20] found a mild correlation between kinematical measures of individual

Table 1 Comparison of demographic characteristics and gait parameters between the groups

	RA group		Control group		P value
	Mean	SD	Mean	SD	
Age (years)	65.9	10.0	69.1	5.8	0.189
Height (cm)	154.3	7.3	154.6	7.5	0.775
Weight (kg)	53.5	9.5	54.4	9.5	0.807
Gender female (n (%))	35 (89.7%)		15 (75.0%)		0.135
Disease duration (years)	11.9	9.4			
DAS (point)	3.2	1.4			
mHAQ (point)t	3.1	3.7			
Walking ability	15.9	4.9			
Walking speed (m/s)	1.03	0.26	1.30	0.54	<0.001
Peak frequency	2.13	0.25	2.03	0.08	0.073
Autocorrelation	0.735	0.122	0.796	0.081	0.037
Coefficient of variance (%)	15.1	10.0	9.2	3.8	0.011

DAS disease activity score, *mHAQ* modified health assessment questionnaire

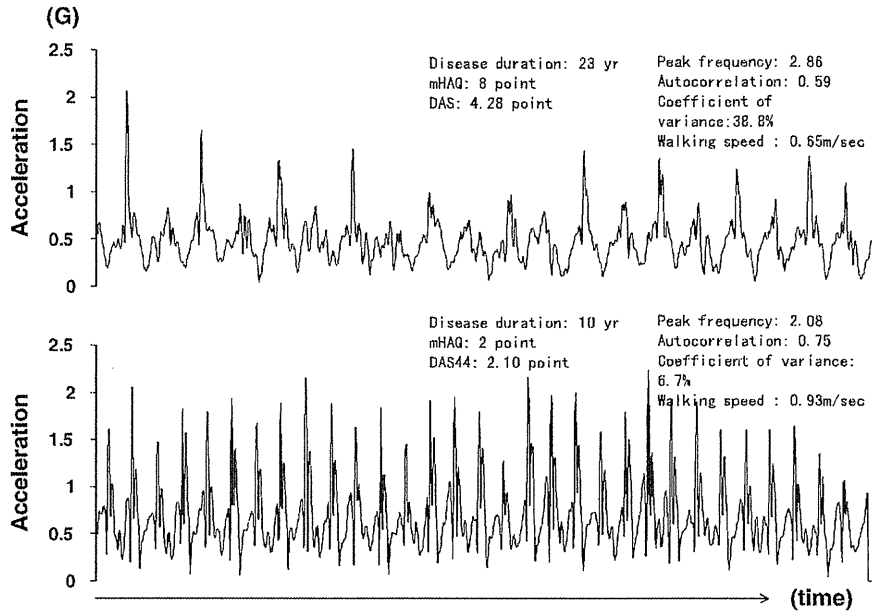

Fig. 2 The waveform of a patient with relatively severe rheumatoid arthritis (*top panel*) is irregular (peak frequency [PF] = 2.86, autocorrelation peak [AC] = 0.59, coefficient of variance [CV] = 38.8%, walking speed = 0.65 m/s). On the other hand, the waveform of a patient with relatively slight disease (*bottom panel*) is regular (PF = 2.08, AC = 0.75, CV = 6.7%, walking speed = 0.93 m/s). *DAS* disease activity score, *mHAQ* modified health assessment questionnaire

Table 2 Spearman's correlation coefficients for gait parameters and clinical parameters

	DAS	mHAQ	Walking ability	Walking speed
Peak frequency	−0.193	0.075	−0.247	0.280*
Autocorrelation	−0.283*	−0.368*	0.257*	−0.704**
Coefficient of variance	0.334*	0.155	−0.420**	0.608**
Walking speed	0.194	−0.442**	0.413**	

DAS disease activity score, *mHAQ* modified health assessment questionnaire

* $P < 0.05$; ** $P < 0.01$

joints and gait speed. Therefore, in systemic illnesses such as RA, it is possible that global waveform analysis is better than local waveform analysis for gait assessment. The results of the present study suggest that assessment of gait parameters using the smartphone is an acceptable method for evaluating gait in RA patients. Indeed, surprisingly, gait parameters measured by the smartphone were found to constitute an index of disease activity and physical function in patients with RA.

Self-management is important not only for patients with RA, but also for patients with other chronic disorders [21, 22]. Pain, disability, fatigue, and self-related general health are improved by systematic self-management educational programmes [21, 22]. Fatigue, especially, is difficult to control by medication and benefits from self-management [23]. The greatest benefit is observed if self-management programmes are maintained for over 8 years [24]. Online self-management systems have been constructed [25], and self-assessed walking ability, such as that described here, may be a useful addition to self-management systems.

The smartphone gait analysis application may be used as a clinical assessment tool and may also potentially be used as a standard method of self-assessment in RA patients, due to several benefits. First, it requires a shorter time for gait assessment in a non-clinical setting compared with traditional assessment tools. Second, it can be used to assess gait patterns easily in daily life. Third, medical practitioners and patients may be able to share information

Table 3 Multiple stepwise regression analysis for gait parameters and clinical parameters

Independent variables	DAS R^2 value = 0.189* Standard regression value	mHAQ R^2 value = 0.135* Standard regression value	Walking ability R^2 value = 0.232** Standard regression value	Walking speed R^2 value = 0.647** Standard regression value
Peak frequency				−0.575**
Autocorrelation	−0.435*	−0.368*		−0.410**
Coefficient of variance			−0.420**	

DAS disease activity score, *mHAQ* modified health assessment questionnaire

* $P < 0.05$; ** $P < 0.01$

phy [11–12]. These reports raise the possibility that some of the 28 joints are less frequently involved, and are less informative for disease activity. Analyses for characterization of joint symptoms would uncover correlations of unexpected joint symptoms and distribution of synovitis in RA.

Here, we analyzed the distribution of affected joints in the 28 joints in patients with RA using more than 17,000 joint assessments from 1,314 patients with RA and showed that synovitis in RA patients can be classified into three groups. We also showed that affected rates of the 28 joints greatly vary in RA patients, and that RA patients could be classified into subgroups based on the distribution of joint synovitis.

Results

Frequency order of joints involvement

We recruited 17,311 assessments for the 28 joints in 1,314 patients with RA from 2005 to 2011. A summary of the registered patients is listed in Table 1. The distribution of the number of patients with RA in each year and the number of joint assessments for each patient are shown in Figure S1. We analyzed how often each of the 28 joints was tender or swollen in patients with RA in 2011. From the analysis of 735 patients, we found that the frequency of joint swelling and tenderness in the 28 joints is widely different from joint to joint (Figure 1 and Table S1). The wrist joints were the most frequently affected joints for swelling and tenderness. The frequency of the right wrist joint being affected was more than four times as high as the least frequently affected joint. Many of the joints showed right-dominant tenderness (eleven of fourteen joints, $p = 0.057$, binomial test), indicating mostly right-handedness. We found strong correlations for the affected rates of each joint between swellings and tenderness except for shoulder joints (Spearman's rank-sum coefficient, rho = 0.70 and $p = 3.8\times10^{-5}$, Figure 1, Table S1). Shoulder joints showed much higher frequencies of tenderness than those of swellings.

Next, we tried to replicate the order of affected frequencies of the 28 joints and the correlation between tenderness and swellings in different RA patients. We obtained 579 patients whose joints data were not available for 2011, indicating we analyzed independent RA patients. We found that the order of the affected joint frequencies were well correlated for both swelling and tenderness among different sets of RA patients (Spearman's rank-sum coefficient, rho:0.815 and 0.904, $p = 1.3\times10^{-7}$ and $p = 4.6\times10^{-11}$ for swelling and tenderness, respectively, Figure S2). We also confirmed that rates of tenderness were well correlated with those of swellings in the 28 joints in the 579 patients (rho:0.604). These results indicate that some of the 28 joints are more likely to develop arthritis than the others in RA patients. The swelling and tenderness correlate with each other except for shoulder joints.

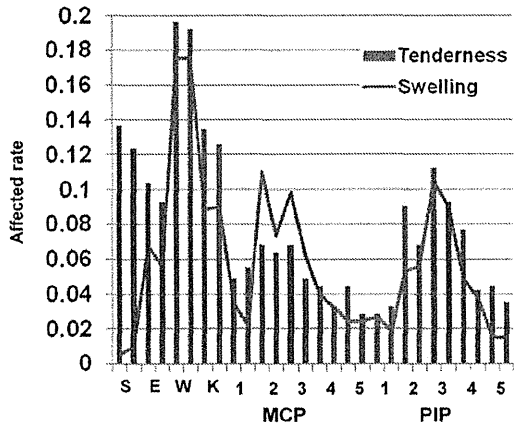

Figure 1. Affected rate of joint symptoms. Affected rate of joint symptoms. Each joint is arranged in the order of right and left. S:shoulder, E:elbow, W:wrist, K:knee.
doi:10.1371/journal.pone.0059341.g001

Table 1. Summary of the KURAMA database.

	The KURAMA database
RA patients	1314
Age (mean±SD)	60.2±15.1
female ratio	81.70%
disease duration (years)	12.2±9.8
Stage*	2.75±1.17
Class*	1.87±0.69

*Stage and Class represent Steinbrocker's stage and class, respectively.
SD: standard deviation.
doi:10.1371/journal.pone.0059341.t001

Whether the right-dominant involvement of joints in patients with RA is associated with joint destruction was analyzed. Joint destruction in the hand was evaluated for 246 patients with RA by modified Sharp score [13]. The six elements of the scores were separately analyzed, namely erosion of PIP, MCP, and wrist joints (we defined as joints other than MCP and PIP in hand) and narrowing of PIP, MCP, and wrist joints. We found that five out of six elements showed right-dominant destruction. In particular, narrowing and erosion of MCP joints showed a statistically significant right-dominance in binomial test ($p <= 0.0050$, Table S2).

Three groups of 28 joints in RA synovitis

Next we analyzed correlations of joint symptoms between the 28 joints. We randomly picked up one assessment from each of the 1,314 patients to maximize the power. When the correlation of tenderness of the 28 joints was analyzed with kappa coefficient, we confirmed that each joint showed a symmetric involvement (Figure 2A). The results also showed that the tenderness of large joints and wrist joints are not correlated with the tenderness of PIP and MCP joints. We found that the tenderness of MCP joints was especially well correlated with each other and that PIP joints tenderness was well correlated with each other. The correlation of swelling in the 28 joints showed the same tendency as that of tenderness, namely, symmetric joint involvement, correlations between large joints and wrist joints, and no strong correlations between wrist joints and other small joints (Figure 2B).

Next we used eigen vectors of principal component analysis to assess the correlations of the 28 joints involvement. When we analyzed correlations of tenderness, eigen vectors revealed that PIP and MCP joints can be clearly distinguished from large joints and wrist joints (Figure 3A). PIP joints and MCP joints turned out to make independent groups after excluding large joints and wrist joints (Figure 3B). These three groups of affected joints were found both for tenderness and swelling (Figure 3C and 3D). We confirmed these three correlation groups in four independent resampling analyses by randomly picking up one assessment from each of the 1,314 patients four times (data not shown). The three groups were observed in the two independent sets of RA patients which were used in the analysis of joints involvement frequency

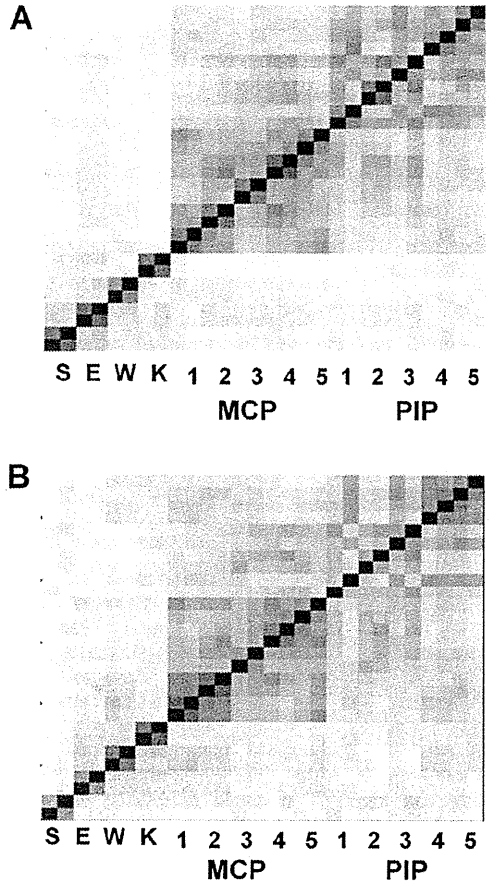

Figure 2. Correlations between the 28 joint symptoms. Brightness of the red color corresponds to the strength of correlations between joint tenderness (A) or swellings (B), using the Kappa coefficient. Each joint is arranged in the order of right and left. The joint order in the y axis is the same as the x axis. The result is a representative of five analyses based on resampled assessments. S:shoulder, E:elbow, W:wrist, K:knee.
doi:10.1371/journal.pone.0059341.g002

(Figure S3). In addition, no significant difference was observed in the relationship of the three groups of joint involvement when we divided the 1,314 patients into two groups according to the patients' caring physicians (Figure S4). We confirmed the three groups by resampling four times for each analysis (data not shown). These results indicate that these three groups were not due to specific patients, examiners, or time of evaluation.

Taken together, the correlation analyses using kappa coefficient and eigen vectors in principal component analysis indicated that there are three correlated groups of joints in RA synovitis, namely, large joints with wrist joints (which we express as "large and wrist joints"), PIP joints, and MCP joints.

Subgroups of patients with RA

We performed a clustering analysis of 5,383 evaluations of 28 joints from 1,314 patients with RA. Six subgroups of evaluations of 28 joints were observed (Figure 4). Each of the subgroups was characterized by 1) no synovitis (34.6%), 2) mild activity with dominant involvement of large and wrist joints (17.4%), 3) dominant involvement of MCP joints (18.3%), 4) dominant involvement of PIP joints (9.3%), 5) active synovitis (4.1%), and 6) moderate activity with dominant involvement of large and wrist joints (16.4%) (Table S3). Whether patients with RA are classified into the same subgroups was analyzed. There were 998 patients with four or five evaluations, and of these, 734 were categorized into the regular groups across different evaluations, indicating that the patterns of synovitis in the same patients were stable. Analysis of joint destruction in each subgroup revealed that the sixth subgroup demonstrated dominant destruction of large and wrist joints compared with MCP and PIP joints ($p<=2.8\times10^{-5}$, Figure S5 and Figure S6).

Discussion

Since RA is a joint destructive autoimmune arthritis and joint damage occurs rapidly in the early stages of the disease course [14], the development of a quantitative scale which assesses disease activity and predicts joint damage is very important. After DAS and ACR core sets were introduced, DAS28, SDAI, and CDAI were developed to evaluate disease activity and easily calculate the disease activity score in patients with RA. All three indices were shown to be well correlated with future joint destruction and they share the same 28 joints for evaluation. Joint symptoms especially joint swelling is known to correlate with future joint damage [3]. While these indices were developed for use in clinical trials such as responsiveness to treatment, they are used by rheumatologists in daily clinical practice and they are reported to coincide very well among different examiners [9]. Characterizing the relative affected frequency of each joint and analysis of correlation between joint symptoms are important to analyze the basic mechanisms of synovitis and to efficiently select the joints to predict future joint destruction. However, there is no detailed analysis to address the correlations between the 28-joint symptoms.

In the current study, we characterized the 28-joint symptoms using large numbers of joint assessments. While we reported the affected rates of each joint in the 28 joints for tenderness and swelling of RA patients registered in the KURAMA database in 2011 as a representative (Table S1), these rates should not be generalized considering large effects of treatment especially biologics agents on joint symptoms. Thus, we focused on relative frequencies of joint involvement for the 28 joints. The affected frequency pattern was compared between the two sets of RA patients, and there were no apparent differences between the two sets for both tenderness and swelling. We also showed that joint symptoms in RA could be classified into three groups both for tenderness and swelling. Our analysis also demonstrated that patients with RA can be regularly classified into six subgroups based on patterns of joint symptoms. These results suggest that regular RA joint involvement pattern, including relative frequency and groups of joints, is largely maintained in RA patients. In addition, we confirmed that these patterns of joint involvement were not attributed to evaluators and fractions of RA patients.

It is interesting that the affected frequencies greatly varied from joint to joint, and the rate of the most highly affected joint was more than four times as high as the least-affected joint. The affected frequencies indicated that wrist joints were the most frequently affected. It should be noted that surface area may have influenced the sensitivity of detecting synovitis in physical exams when different joints were compared. The relatively high frequency of tenderness and swelling in large and wrist joints compared with MCP and PIP joints can be explained by this difference in surface area. However, surface area cannot fully explain the highest frequency of wrist involvement and different frequencies within the MCP or PIP joints. A dominant involve-

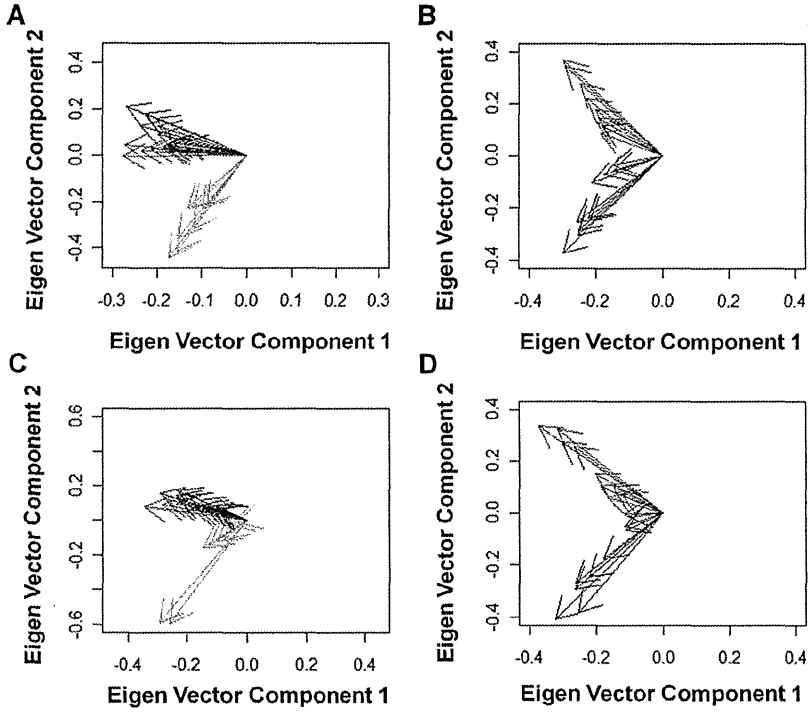

Figure 3. Relationship of the 28-joint involvement. The 1st and 2nd components of eigen vectors of the joint symptoms are plotted, using principal component analysis of the 28 joint involvement for tenderness (A) and swelling (C) or using that of the 20 joint involvement other than large and wrist joints for tenderness (B) and swelling (D). The results are representatives of five analyses based on resampled assessments. Green: large and wrist joints. Red: MCP joints. Blue: PIP joints.
doi:10.1371/journal.pone.0059341.g003

ment of right joints seemed to indicate a majority of the study population being right-handed in spite of the small difference of affected rates between bilateral joints. We also demonstrated that the right dominant involvement was also true for joint destruction. We could not compare the joint involvement and joint destruction between right-handed patients and left-handed patients due to a lack of information regarding handedness of patients.

Correlation analysis confirmed the well-known symmetric joint involvement in patients with RA. Strong correlations of tenderness and swelling in the same joints except for shoulder joints may indicate low sensitivity of shoulder swelling in the physical exams and common mechanisms of swelling and tenderness. It is striking that joint symptoms can be classified into three groups based on correlation analysis and principal component analysis. The association observed between the symptoms in the wrist joints and the large joints is worth noting, since wrist joints are regarded as small joints according to ACR/EULAR criteria set in 2010. As wrist joints are much closer to other small joints than large joints, the relationship between wrist joints and large joints cannot be explained by the distance of joints. The distance of joints cannot explain the two different groups of MCP and PIP joints either. While symptoms of large and wrist joints are not related with those of MCP and PIP joints, they were not very strongly correlated with each other, compared with correlations among PIP joints or MCP joints. This may indicate that there are no common strong factors which predispose large and wrist joints to swelling and tenderness in patients with RA.

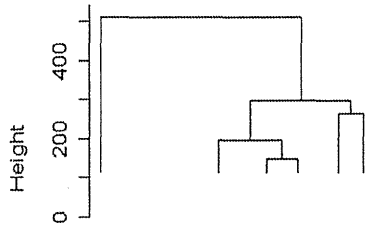

Figure 4. Six subgroups of evaluations of the 28 joints in RA. Results of clustering analysis with Ward method using randomly obtained 5,383 evaluations of the 28 joints in 1,314 patients were plotted.
doi:10.1371/journal.pone.0059341.g004

We also showed that patients with RA can be divided into six subgroups based on these three groups of joint involvement. More than 70% of patients are classified into regular subgroups, indicating that the pattern of synovitis in a patient with RA is stable. When patients who were regularly classified into the first subgroup of patients characterized by no synovitis were removed, more than 60% of patients were still classified into regular subgroups (data not shown), indicating that the stable patterns were observed regardless of activity of RA. As joint destruction was influenced by disease duration, disease activity, and treatment, we analyzed the relative distribution of joint destruction between the three joint groups in a patient with RA. We found that the sixth subgroup of patients, characterized by moderate activity with dominant involvement of large and wrist joints, demonstrated dominant destruction of wrist joints. This suggests that classifying patients with RA into appropriate subgroups would lead to prediction of patterns of joint destruction.

There are reports that evaluating fraction of joints by ultrasonography is a good way to predict future joint damage [11–12]. One study reported that 5 of the 28 joints with MTP2 and MTP5 joints, namely, wrist, MCP2, MCP3, PIP2, and PIP3 joints, are enough for ultrasonography evaluation [12]. Their data seems to be consistent with our results as they selected at least two joints from three different groups into which the 28-joint symptoms were classified. As ultrasonography usually surpasses physical examination in terms of the sensitivity to detect synovitis, it is interesting to analyze whether the assessments of synovitis using ultrasonography show the same pattern of synovitis over the 28 joints in RA.

Our results indicate that RA does not develop synovitis in the 28 joints with the same frequency and that the affected rate of each joint greatly varies from joint to joint. These different distributions of joint synovitis would lead to different distribution of joint destruction. Based on our results, the 28 joints can be categorized into three groups, and it is possible that some fractions of the 28 joints are less informative to assess disease activity than others. It would be interesting to develop a novel simplified joint core set, and analyze the correlation between joint damage and activity score based on this. It would be also interesting to characterize each of RA subsets in more detail.

Materials and Methods

Ethics Statement

Written informed consent to enroll in the database described below was obtained from most of the patients, but for some patients the information regarding the construction of this database was disclosed instead of obtaining written informed consent. Participants who were informed regarding the construction of the database (instead of obtaining written informed consent) were allowed to withdraw from the study if desired.

All data were de-identified and analyzed anonymously. This study was designed in accordance with the Helsinki Declaration. This study including the consent procedure was approved by the ethics committee of Kyoto University Graduate School and Faculty of Medicine.

The KURAMA database

The KURAMA (Kyoto University Rheumatoid Arthritis Management Alliance) database was established in 2011 at Kyoto University to store detailed clinical information and specimens from patients with arthritis and arthropathy. The alliance is composed of rheumatic disease-associated departments in Kyoto University Hospital as well as its allied, integrating previous database and specimen collections in each department and allied. A template for electronic clinical charts developed at Kyoto University Hospital in 2004 to evaluate joint involvements in RA patients was used to obtain joint assessments. Rheumatologists evaluated swelling and tenderness of the 28 joints in patients with RA on each visit and filled in the template. The synovitis information of the 28 joints and data for C-reactive protein and erythrocyte sedimentation rate were extracted from electronic clinical charts [15] and stored in the KURAMA database.

Patients and data of joint assessment

A total of 17,311 joint assessments from 1,314 patients with RA from 2005 to 2011 were obtained in a retrospective manner from the KURAMA database. All of the patients fulfilled ACR revised criteria for RA in 1987 [10] or ACR and EULAR classification criteria for RA in 2010 [16–17].

Analysis of affected frequencies in the 28 joints

RA patients were subdivided depending on whether their data were available in 2011 or not, and the affected frequency in each of the 28 joints was calculated. We compared the order of the affected frequency in the 28 joints between the two patient sets with Spearman's rank-sum coefficient. We separately analyzed the affected rates of joints for swelling and tenderness. When multiple joint assessments in different visits were available in the same patient with RA, we randomly selected one of the assessments as representative in the patient. We compared frequencies between tenderness and swellings for the 28 joints with Spearman's rank-sum coefficient.

Clustering of patients with RA

Clustering analyses were performed by Ward method, using randomly-selected 5,383 evaluations of the 28 joints from 1,314 patients with RA. These evaluations did not contain more than six assessments from each patient to avoid excess influence of particular patients. Affected rates were calculated for the three groups of joints (namely PIP joints, MCP joints and large and wrist joints) in this clustering analysis. For example, when a patient showed tenderness and swelling for all PIP joints, the affected rate of PIP joints in the patient is 2. When a patient showed tenderness for four MCP joints, the affected rate of MCP joints is 0.4.

RA patients were regarded as belonging to a particular group when more than 60% of evaluations belonging to the same patients with four or five evaluations were classified into the same group.

Analysis between RA subgroups and joint destruction

Joint destruction of hand joints in 246 patients with RA was evaluated by modified Sharp score by a trained rheumatologist who was not informed of the patients' characteristics (KM). Joint destruction rates were defined for the three groups of joints as a sum of scores divided by the full score in the joints group. For example, when a patient shows 50 as a sum of scores in the large and wrist group, the patient's joint destruction rate for the group is 0.463 (50/108).

Correlation of the 28 joints and statistical analysis

Correlations of joint symptoms among the 28 joints were estimated separately for tenderness and swelling. We randomly obtained one assessment of the 28 joints in each patient as a representative of the patient's joint assessments for maximization of the power. Kappa coefficient was used to analyze coincidence of joint symptoms in each pair of the 28 joints. Eigen vectors obtained in principal component analysis were used to analyze the deviation of joint symptoms. We resampled joint assessments for each patient and created four other sets of joint assessments. The same correlation analyses were performed using the four resampled assessments to confirm the correlation shown in the first assessment set. Right dominance of the synovitis and joint destruction was analyzed by binomial test. Dominant destruction of joints was evaluated by paired-t test. Statistical analysis was performed by R software or SPSS (ver18).

Supporting Information

Figure S1 Distribution of joint evaluation counts and patients across different years. A) Distribution of number of RA patients according to numbers of 28-joint assessments. B) Distribution of number of patients with RA whose joint assessment data were available from 2005 to 2011 in the KURAMA database. (TIF)

Figure S2 Good correlations between joint involvement rates in different sets of RA patients. Rates of joint involvement for A) swelling and B) tenderness were compared between the two different sets of RA patients. X and Y axes represent rates in the first set of RA patients in 2011 and those in the second set in 2005 to 2010, respectively.
(TIF)

Figure S3 Three groups of joints regardless of different sets of RA patients. Analysis using one of four resampled assessments in one of the two sets of RA patients is shown as a representative. The 1st and 2nd components of eigen vectors of the joint symptoms are plotted, using principal component analysis of the 28 joint involvement for tenderness (A) and swelling (C) or using that of the 20 joint involvement other than large and wrist joints for tenderness (B) and swelling (D). Green: large and wrist joints. Red: MCP joints. Blue: PIP joints.
(TIF)

Figure S4 Three groups of joints regardless of different evaluators. Analysis using one of five resampled assessments by one of the two groups of medical doctors is shown as a representative. The 1st and 2nd components of eigen vectors of the joint symptoms are plotted, using principal component analysis of the 28 joint involvement for tenderness (A) and swelling (C) or using that of the 20 joint involvement other than large and wrist joints for tenderness (B) and swelling (D). Green: large and wrist joints. Red: MCP joints. Blue: PIP joints.
(TIF)

Figure S5 Dominant destruction of large and wrist joints in the sixth subgroup of patients with RA. Box plots indicating the joint destruction rates in the three joint groups in subjects belonging to the sixth subgroup.
(TIF)

Figure S6 Destruction of large and wrist joints among the six subgroups of RA. Differences in destruction rates were plotted for each subject in the six subgroups. The difference was defined as: A) destruction rate of group of large and wrist joints – destruction rate of MCP joints and B) destruction rate of group of large and wrist joints – destruction rate of PIP joints.
(TIF)

Table S1 Rate of joint involvement for 28 joints in RA.
(DOC)

Table S2 Right-dominant joint destruction in RA. Patients who showed unilateral higher or lower scores in each element were analyzed.
(DOC)

Table S3 Mean affected rates of the three joint groups in the six subgroups of patients with RA.
(DOC)

Acknowledgments

We would like to thank to Mr. Wataru Yamamoto at Kurashiki Kosai Hospital for his excellent support to establish and maintain the KURAMA database. We also thank Drs Hisashi Yamanaka, Katsunori Ikari, and Ayako Nakajima at Institute of Rheumatology, Tokyo Women's Medical University for their kind instruction and advice for management of rheumatic diseases database.

Author Contributions

Evaluation of joint X-rays: KM. Conceived and designed the experiments: CT MH KO RY FM HI TF TM. Analyzed the data: CT. Contributed reagents/materials/analysis tools: CT MH KO RN KM N. Yamakawa H. Yoshifuji N. Yukawa DK TU H. Yoshitomi MF HI TF TM KY. Wrote the paper: CT.

References

1. Firestein GS (2003) Evolving concepts of rheumatoid arthritis. Nature 423: 356–361.
2. Drossaers-Bakker KW, de Buck M, van Zeben D, Zwinderman AH, Breedveld FC, et al. (1999) Long-term course and outcome of functional capacity in rheumatoid arthritis: the effect of disease activity and radiologic damage over time. Arthritis and Rheumatism 42: 1854–1860.
3. Smolen JS, Van Der Heijde DM, St Clair EW, Emery P, Bathon JM, et al. (2006) Predictors of joint damage in patients with early rheumatoid arthritis treated with high-dose methotrexate with or without concomitant infliximab: results from the ASPIRE trial. Arthritis and Rheumatism 54: 702–710.
4. Felson DT, Anderson JJ, Boers M, Bombardier C, Chernoff M, et al. (1993) The American College of Rheumatology preliminary core set of disease activity measures for rheumatoid arthritis clinical trials. The Committee on Outcome Measures in Rheumatoid Arthritis Clinical Trials. Arthritis and Rheumatism 36: 729–740.
5. van der Heijde DM, van 't Hof MA, van Riel PL, Theunisse LA, Lubberts EW, et al. (1990) Judging disease activity in clinical practice in rheumatoid arthritis: first step in the development of a disease activity score. Annals of the Rheumatic Diseases 49: 916–920.
6. van der Heijde DM, van't Hof MA, van Riel PL, van Leeuwen MA, van Rijswijk MH, et al. (1992) Validity of single variables and composite indices for measuring disease activity in rheumatoid arthritis. Annals of the Rheumatic Diseases 51: 177–181.
7. Smolen JS, Breedveld FC, Schiff MH, Kalden JR, Emery P, et al. (2003) A simplified disease activity index for rheumatoid arthritis for use in clinical practice. Rheumatology 42: 244–257.
8. Aletaha D, Smolen JS (2007) The Simplified Disease Activity Index (SDAI) and Clinical Disease Activity Index (CDAI) to monitor patients in standard clinical care. Best Pract Res Clin Rheumatol 21: 663–675.
9. Salaffi F, Cimmino MA, Leardini G, Gasparini S, Grassi W (2009) Disease activity assessment of rheumatoid arthritis in daily practice: validity, internal consistency, reliability and congruency of the Disease Activity Score including 28 joints (DAS28) compared with the Clinical Disease Activity Index (CDAI). Clinical and Experimental Rheumatology 27: 552–559.
10. Arnett FC, Edworthy SM, Bloch DA, McShane DJ, Fries JF, et al. (1988) The American Rheumatism Association 1987 revised criteria for the classification of rheumatoid arthritis. Arthritis Rheum 31: 315–324.
11. Scheel AK, Hermann KG, Kahler E, Pasewaldt D, Fritz J, et al. (2005) A novel ultrasonographic synovitis scoring system suitable for analyzing finger joint inflammation in rheumatoid arthritis. Arthritis and Rheumatism 52: 733–743.
12. Backhaus M, Ohrndorf S, Kellner H, Strunk J, Backhaus TM, et al. (2009) Evaluation of a novel 7-joint ultrasound score in daily rheumatologic practice: a pilot project. Arthritis and Rheumatism 61: 1194–1201.
13. van der Heijde D (2000) How to read radiographs according to the Sharp/van der Heijde method. Journal of Rheumatology 27: 261–263.
14. Machold KP, Stamm TA, Eberl GJ, Nell VK, Dunky A, et al. (2002) Very recent onset arthritis – clinical, laboratory, and radiological findings during the first year of disease. Journal of Rheumatology 29: 2278–2287.
15. Yamamoto K, Yamanaka K, Hatano E, Sumi E, Ishii T, et al. (2012) An eClinical trial system for cancer that integrates with clinical pathways and electronic medical records. Clin Trials 9: 408–417.
16. Aletaha D, Neogi T, Silman AJ, Funovits J, Felson DT, et al. (2010) 2010 Rheumatoid arthritis classification criteria: an American College of Rheumatology/European League Against Rheumatism collaborative initiative. Arthritis and Rheumatism 62: 2569–2581.
17. Aletaha D, Neogi T, Silman AJ, Funovits J, Felson DT, et al. (2010) 2010 rheumatoid arthritis classification criteria: an American College of Rheumatology/European League Against Rheumatism collaborative initiative. Annals of the Rheumatic Diseases 69: 1580–1588.

KOKUYO セホ-50B